Earthquake Detection and P-Wave Arrival Time Picking Using Capsule Neural Network

Omar M. Saad and Yangkang Chen

Abstract—Earthquake detection is an essential step in observational earthquake seismology. We propose to utilize a capsule neural network (CapsNet) to automatically identify and detect earthquakes. CapsNet is the new generation of deep learning architecture. It has the capability of learning with a great generalization performance from a small dataset. We train the CapsNet using 50% of the Southern California seismic data (2.25 million 4-s-three-component seismic windows) and use 222 395 waveforms from different seismic areas to evaluate the CpasNet performance, e.g., western United States, Europe, and Japan. As a result, the CapsNet misses 367 events and detects 217 305 events with an accuracy of 97.71%. Among these picked events, 210 498 events have an arrival time error below 0.2 s (96.86%) and 197 968 waveforms with an arrival time error below 0.1 s (91.11%). The CapsNet precision, recall, and F1-score are 97.78%, 99.83%, and 98.79%, respectively. In addition, the CapsNet is tested using 100 000 60-s-three-component seismic noise waveforms. CapsNet shows a low false alarms rate of 1384, which gives the CapsNet an accuracy of 98.61%. In addition, CapsNet is tested using continuous seismic data associated with the 24-hours microearthquakes swarm that occurred in the Arkansas area. Accordingly, the CapsNet detects 221 earthquakes and releases 37 false alarms with a detection accuracy of 85.65%. CapsNet detects many microearthquakes with a small magnitude, as low as −1.3 Ml, and detects earthquakes that have a low signal-to-noise ratio (SNR), e.g., as low as −8.07 dB. The results of the CapsNet are compared to the benchmark methods, e.g., short-time average/long-time average (STA/LTA) and GPD methods. The CapsNet shows the highest picking accuracy and outperforms the benchmark methods.

Index Terms—Capsule neural network (CapsNet), earthquake detection, machine learning.

I. INTRODUCTION

IDENTIFICATION and detection problems of the earthquake are the key roles in several seismology analyses, e.g., magnitude estimation, hypocenter location, and other parameters that are utilized to build the seismic catalogs. Hand-picking becomes difficult and unreliable due to the increase of seismogram database volume, the occurrence of the earthquake swarm with small-magnitude earthquakes, and

Omar M. Saad is with the Key Laboratory of Geoscience Big Data and Deep Resource of Zhejiang Province, School of Earth Sciences, Zhejiang University, Hangzhou 310027, China, and also with ENSN Laboratory, Seismology Department, National Research Institute of Astronomy and Geophysics (NRIAG), Egypt (e-mail: omar.saad@nriag.sci.eg).

Yangkang Chen is with the Key Laboratory of Geoscience Big Data and Deep Resource of Zhejiang Province, School of Earth Sciences, Zhejiang University, Hangzhou 310027, China (e-mail: chenyk2016@gmail.com).

the existence of a large amount of background noise. Hence, automatic algorithms should be applied to identify and detect earthquakes.

Short-time average/long-time average (STA/LTA) is a commonly used algorithm in the detection and identification of the earthquakes [1]. However, STA/LTA suffers from several drawbacks, e.g., inaccurate initialization parameters lead to several false alarms, and it does not perform well with the existence of a large amount of noise. In addition, the Akaike information criterion (AIC) is one of the benchmark algorithms used widely in the earthquake detection problem [2]. However, AIC estimates the global minimum incorrectly when the background noise level becomes high. On the other hand, another group of automatic detection methods has been proposed to detect the earthquakes based on machine learning techniques, e.g., K-means algorithm [3], [4], template matching [5], [6], support vector machine [7], fuzzy algorithm [8], wavelet transformation [9], and thresholding algorithm [10].

Recently, deep learning has become a powerful tool in the field of seismology [11]–[24]. Several deep learning techniques based on convolutional neural network (CNN), deep recurrent neural network (RNN), and autoencoder have been proposed to detect the earthquakes [25]–[32]. CNN shows a great ability to extract significant features from the input data. However, it suffers from several drawbacks. One of the main layers in CNN architecture is the pooling layer which reduces the dimensionality of the network. However, the pooling layer could lose some important information, which limits the performance of the network [33]. Also, CNN does not care about the relative spatial relationships between the extracted features, which makes the generalization ability not robust enough [34]. The CNN is translationally invariant and also has invariance to a small degree of rotation [35]. On the other hand, the capsule network (PickCapsNet) is utilized to detect the P-wave arrival time of the microseismic data [36]. However, PickCapsNet has several pooling layers that leads to the same problem of the CNN (losing some important information).

Capsule neural network (CapsNet) is first introduced by Sabour *et al.* [33] to overcome the drawbacks of the CNN. CapsNet is the new generation of the deep learning architecture that gives the ability of the network to learn without the pooling layer (without losing information), train with fewer samples data, and obtain generalization ability and a robust classification performance due to its vector output based on simpler network architecture.

All the abovementioned advantages of the CapsNet can be utilized in the earthquake detection problem. We can train

a simple CapsNet architecture with a small dataset size, which can lead to great generalization ability for earthquake detection. Therefore, we propose to use CapsNet to classify between the noise and the earthquake signals. Afterward, we detect precise P-wave arrival time. CapsNet is trained using the open-source data recoded by Southern California seismic stations [26] and tested on several earthquakes in Asia and Europe. The results are promising and better than those from the benchmark algorithms, e.g., STA/LTA [1] and GPD [26] methods.

II. METHODOLOGY

A. Framework of CapsNet

The proposed algorithm consists of two steps: first, identifying the earthquakes signals by checking the existence of both P- and S-waves. If both phases exist, we consider these signals as an earthquake and, second, extracting the P-wave arrival time of the event. To achieve such a task, we use the Southern California dataset [26] to train the CapsNet. This dataset contains 4.5 million 4-s-three-component seismic windows: 1.5 million P-wave seismograms, 1.5 million S-wave seismograms, and 1.5 million noise seismograms. The P- and S-waves are centered on each window, i.e., the arrival times of P- and S-waves are located after 2 s from the window start time. All the noise windows have a label of zero, while the P- and S-waves' windows have a label of one. We randomly split the Southern California dataset into 50% for training, 25% for validation, and 25% for testing. For the continuous data, the input seismic record is divided into several 4-s-three-channel overlapped windows, i.e., the window moves by ten samples. Afterward, if the CapsNet finds the two phases (P- and S-waves), it is considered as an event; otherwise, it is considered as noise. Finally, in the case of identifying an event, the P-wave arrival time is estimated.

B. CapsNet Architecture

CapsNet consists of three main layers: convolutional, primary capsule, and digit capsule layer. First, the convolutional layer is used to extract the significant features from the input data. We use two convolutional layers, each having 64 and 128 feature maps, respectively. The output of each feature map can be determined as follows:

$$y(i, j) = \sum_{m=-N}^{N} \sum_{n=-M}^{M} x(i + m, j + n) * k(m, n) \quad (1)$$

where x is the input of the convolutional layer, k is the kernel (filter), and N and M are the kernel sizes. In our case, the input has a size of $400 \times 3 \times 1$, and we use a kernel size of 3×3 and the kernel strides with one sample. Rectified linear unit (ReLU) is used as an activation function after each convolutional layer that has an output as follows:

$$\text{Act}(y) = \max(0, y) \quad (2)$$

Second, for the primary capsule, the output of the convolutional feature maps is split into several vector representations named capsules (u_i) to produce combinations of the features. Capsule behavior is similar to convolutional layer,

i.e., it applies a convolutional operation to their input. We use a kernel size of 3×3 and the kernel strides with 3 samples. Capsule contains all the information about the input data including orientation and position. Here, we use four capsules, each having 16 channels. Thus, the output of the capsule layer has a shape of $134 \times 1 \times 16 \times 4$. The output of the capsule is a vector such that the traditional activation function cannot be utilized. Thus, a nonlinear squashing function is used as follows:

$$v_j = \frac{\|s_j\|^2}{1 + \|s_j\|^2} \frac{s_j}{\|s_j\|^2} \quad (3)$$

where s_j and v_j are the input and the output of the capsule j, respectively. The squashing activation function is proposed to ensure that short vectors get shrunk to almost zero length, and long vectors get shrunk to a length slightly below 1 [37]. Third, the digit capsule layer has a 2-D shape. In our problem, we have two classes: noise and earthquake classes. The primary capsule are connected to the digit capsule based on routing by agreement concept (dynamic routing) [33]. s_j can be expressed as a weighted sum over all output contributions ($\hat{u}_{j|i}$). s_j can be determined as follows:

$$s_j = \sum_i c_{ij} \hat{u}_{j|i} \quad (4)$$

where c_{ij} is the coupling coefficient in the dynamic routing algorithm [37]. $\hat{u}_{j|i}$ and c_{ij} can be obtained as follows:

$$\hat{u}_{j|i} = W_{i_j} . u_i \quad (5)$$

$$c_{ij} = \frac{\exp(b_{ij})}{\sum_c \exp(b_{ic})} \quad (6)$$

where W_{i_j} denotes the weight matrix, and b_{ij} and b_{ic} are the log prior probabilities between two capsules. The routing algorithm is an iterative method based on several steps. First, for all capsules in layer l and capsule j in layer $l + 1$, b_{ij} is initialized to be zero, while the weight matrix W_{i_j} is randomly initialized. Second, the coupling coefficient c_{ij} is obtained according to (6). Third, s_j and v_j are obtained based on the coupling coefficient c_{ij} and the capsule output contribution ($\hat{u}_{j|i}$) [computes (3) and (4)]. Finally, b_{ij} is updated as follows:

$$b_{ij} + (\hat{u}_{j|i} . v_j) \rightarrow b_{ij} \quad (7)$$

The output of the digit capsule has a shape of 2×8. Each class can be represented in a vector of eight dimensions. We use three iterations for the routing algorithm. Adam optimizer [38] is used to optimize the CapNet network parameters by minimizing the margin loss function

$$L_k = T_k \max(0, m^+ - \|v_k\|)^2 + \lambda(1 - T_k)\max(0, \|v_k\| - m^-)^2 \quad (8)$$

where T_k equals 1, $m^+ = 0.9$, and $m^- = 0.1$. λ denotes the downweighting of the loss, which is set to be 0.5. The architecture of the proposed algorithm is shown in Fig. 1.

III. EXAMPLES

A. Training Dataset

To train the CapNet, we use the open-source dataset in [26], which consists of 273 882 earthquakes recorded by the Southern California Seismic Network (SCSN) at 692 broadband and
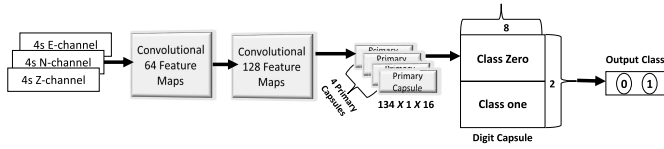
Fig. 1.   CapsNet architecture for the earthquake detection problem.

Classified as	Noise	Earthquake
Noise	389,626 (TN)	10,818 (FP)
Earthquake	8,105 (FN)	784,889 (TP)

short-period three-component stations from 2000 to 2017. The magnitude range of this dataset varies from −0.81 to 5.7 Ml. These earthquakes are divided into 4-s windows, such that the P- and S-waves are centered in the middle of the window. Accordingly, 1.5 million noise windows, 1.5 million P-wave windows, and 1.5 million S-wave windows are extracted to train the network [26]. The P- and S-waves arrival times were manually picked by the SCSN analysts [26]. Each window has a label: zero for noise windows and one for P- and S-waves' windows. We randomly split the dataset into 50% for training, 25% for validation, and 25% for testing, i.e., the CapsNet is trained using 2.25 million 4-s-three-channel seismograms and validated and tested using 2.25 million 4-s-three-channel seismograms. The training dataset is balanced, i.e., the number of outputs having labels of zero is equal to the number of outputs having labels of one.

The training process is stopped if the validation accuracy did not increase for five consecutive epochs or the number of epochs reaches 20. We use a batch size of 1024. The training accuracy reaches 98.75%, while the validation accuracy is 98.42%. We test the remaining 25% of the dataset using the obtained CapsNet model from the training process. As a result, the accuracy of the test dataset is 98.40%. To evaluate the performance of the CapsNet, we obtain the precision, recall, and F1-score as follows:

$$\text{Precision} = \frac{TP}{TP + FP}$$
$$\text{Recall} = \frac{TP}{TP + FN}$$
$$\text{F1} - \text{score} = 2 \times \left(\frac{\text{precision} \times \text{recall}}{\text{precision} + \text{recall}} \right) \qquad (9)$$

where TP, FP, FN, and TN are the true positive, false positive, false negative, and true negative, respectively. The positive and negative represent the earthquake signal and the background noise classes, respectively. Accordingly, for the test dataset, the precision, recall, and the F1-score are 98.64%, 98.98%, and 98.80%, respectively.

Afterward, we obtain the receiver operating characteristic (ROC), as shown in Fig. 2(a), and the area under the ROC curve (AUC) is 0.981. The ROC curve and the AUC value indicate a high classification performance for the CapsNet. The CapNet has two outputs: one for the noise class and the other for the earthquake class. We obtain the recall–precision curve for the earthquake class, as shown in Fig. 2(b). It shows the precision versus the recall values using different threshold values. We can conclude that using a threshold of 0.8 is the optimal choice for detecting the earthquake class and its corresponding P-wave arrival time. The confusion matrix is listed in Table I using a threshold of 0.8.
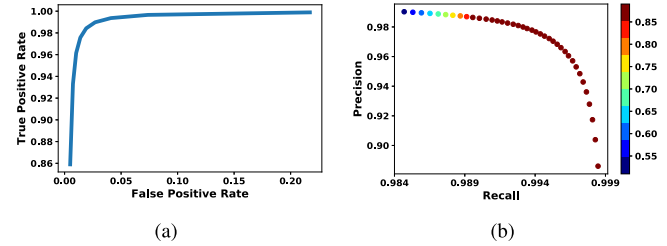

Fig. 2.   Results evaluation of the test sets. (a) ROC. (b) Recall–precision curve for earthquake class.

B. Applying CapsNet to Continuous Seismic Record

For each seismic record, in the case of a 100-Hz sampling rate, the three-channel input data is bandpass filtered between 2 and 20 Hz, normalized and divided into several overlapping windows, each window having a size of 4 s (400 samples in case of 100-Hz sampling rate), while the window moves every ten samples. We bandpass filtered the input data between 2 and 20 Hz because most of the tested events are local events. However, we tried to bandpass filtered the input data between 1 and 40 Hz, and the CapsNet worked well with the same accuracy. For each window, CapsNet determines the output probability of each class (noise and earthquake class). Then, we search for two consecutive peaks in the output probability of the earthquake class to obtain the first arrival time of the event. We search for the probability higher than the predefined threshold and find the maximum peak (maximum probability value) between the predefined threshold and the probability value of 0.1, e.g., if the probability index P_0 has a value of the predefined threshold and the probability index P_1 has a probability value of 0.1, we search for the maximum probability value between the two indices P_0 and P_1. Afterward, we search for the second peak with the same methodology. If we found two peaks, it indicates that this record contains P- and S-waves; hence, this record contains an event. Finally, the corresponding time of the maximum value of the first peak above the predefined threshold (i.e., 0.8) is set to be the first arrival time of the event. Fig. 3 shows an example of the CapsNet output and the first arrival time of the event corresponding to the manual solution and the CapsNet.

C. Southern California Seismic Data

To evaluate the performance of the CapsNet, we use the open-source dataset STEAD [39]. First, we use the earthquake waveforms recorded by the Southern California seismic network in STEAD. All the STEAD waveforms are 60-s-three component seismograms. Accordingly, 8633 waveforms are used to evaluate the CapsNet performance. The magnitude of these earthquakes varies between 0 and 5.42 Ml, while the depth range is 0–34.29 km. The event distance range varies
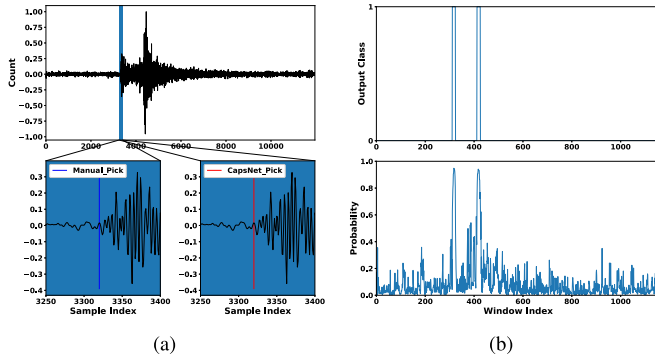
Fig. 3. Example of CapsNet picks from Japan seismic area. (a) Input seismic trace (Z-component) and first arrival pick corresponding to the manual solution and CapsNet. (b) Final output class of the CapsNet (upper figure) and the CapsNet output probability of the earthquake class (lower figure). Note that the output class of the CapsNet is obtained based on the CapsNet output probability. If the output probability exceeds the predefined threshold, the output class is set to be one, and vice versa.

from 0.12 to 329.12 km. The locations of these events are shown in Fig. 4. Each waveform is bandpass filtered between 2 and 20 Hz and divided into several overlapping 4-s-three-component windows. The CapsNet first identifies the existence of an earthquake and then picks the first arrival time of the event. We define the accuracy of the CapsNet as follows:

$$\text{Acc} = \frac{E_0}{E_t} \tag{10}$$

where E_0 is the number of the correct picked events that have a mean absolute first arrival time error below 0.5 s (compared with the manual pick) and E_t is the total number of tested events. As a result, the CapsNet identifies and picks 8331 events with picking error below 0.5 s and misses 57 events. In this case, the accuracy of the CapsNet is 96.50%. The number of picked events that have a picking error below 0.2 s is 7924 (95.11% from the correct picked events), while 7280 events have a picking error below 0.1 s (87.38% from the correct picked events). The probability distribution function (PDF) of the arrival time error corresponding to Southern California Seismic data is shown in Fig. 5(a). We consider the CapsNet picks having a picking error below 0.5 s as the true positive, while the other CapsNet picks are considered as false positive. The missing events are considered as a false negative. Accordingly, for this dataset, the precision, recall, and F1-score are 97.14%, 99.32%, and 98.22%, respectively. In addition, the differences between the CapsNet picks and the manual picks have a mean value, standard deviation, mean absolute error, and mean absolute percentage error of −0.017 s, 0.079 s, 0.042 s, and 1.047%, respectively.

D. Western United States Seismic Data

We use the STEAD earthquake waveforms recorded by the plate boundary observatory (PBO) borehole seismic network. PBO is employed to cover the active boundary zone between the Pacific and North American plates in the western United States. We use 196 986 waveforms with magnitude range between −0.3 and 5.7 Ml and depth range of 0–86.71 km. The event distance range varies from 0.04 to 344.37 km. The locations of these events are shown in Fig. 4. CapsNet detects 193 368 events with arrival time error below 0.5 s (accuracy of

98.16%) and misses 181 events. Among them, 188 823 events have an arrival time error below 0.2 s (97.62% from the correct picked events), while 178 911 events have an arrival time error below 0.1 s (92.50% from the correct picked events). The PDF of the arrival time error corresponding to western United States seismic data is shown in Fig. 5(b). The precision, recall, and F1-score are 98.25%, 99.90%, and 99.06%, respectively. The differences between the CapsNet picks and the manual picks have a mean value, standard deviation, mean absolute error, and mean absolute percentage error of −0.007 s, 0.064 s, 0.039 s, and 0.89%, respectively.

E. European Seismic Data

To evaluate the generalization of CapsNet, we use the STEAD seismic data recorded by the European seismic networks. Among STEAD data, we found 14 488 waveforms recorded by European seismic networks with a magnitude range of 0.3–6.1 Ml, and the depth varies from 0 to 184.07 km. The event distance range varies from 0.13 to 333.39 km. Fig. 4 shows the plots of the locations of these events. Each input seismic record is bandpass filtered between 2 and 20 Hz and divided into several 4-s-three-component windows. CapsNet obtains a label for each window and classifies between the noise and earthquake signals. As a result, CapsNet identifies 13 358 events with arrival time error below 0.5 s (accuracy of 92.20%), 11 609 events with arrival time error below 0.2 s (86.90% from the correct picked events), and 9926 events with arrival time error below 0.1 s (74.30% from the correct picked events), and misses 129 events. The PDF of the arrival time error corresponding to European seismic data is shown in Fig. 5(c). The differences between the CapsNet picks and the manual picks have a mean value, standard deviation, mean absolute error, and mean absolute percentage error of −0.011 s, 0.133 s, 0.081 s, and 2.13%, respectively. The precision, recall, and F1-score are 93.03%, 99.04%, and 95.94%, respectively. Table II summarizes the CapsNet picking results using different seismic areas.

F. Japanese Seismic Data

For further evaluation of the CapsNet generalization performance, we use the earthquakes recorded by station TOWH in Japan during 2014. We use the picks provided by the National Research Institute for Earth Science and Disaster Resilience and Japan Meteorological Agency [40]. The event distance range varies from 13.53 to 112.34 km. The magnitude of the tested events is below 2 Ml, and their depth varies from 0 to 143 km. Accordingly, 2288 waveforms are used to test the performance of the CapsNet. These events are located in the seismic map of Fig. 4. As a result, 2248 waveforms detected below 0.5-s arrival time error, which gives a CapsNet accuracy of 98.25%. Among the correctly detected waveforms, 2142 waveforms have an arrival time error below 0.2 s (95.28% from the correct picked events) and 1851 events have an arrival time error below 0.1 s (82.33% from the correct picked events). Furthermore, we compare the CapsNet result with benchmark algorithms, e.g., STA/LTA [1] and GPD [26] methods. STA/LTA has a picking accuracy of 72.84% (1666 waveforms have a picking error below 0.5 s), while 1320 and 938 waveforms have an arrival time error below 0.2 and 0.1 s,
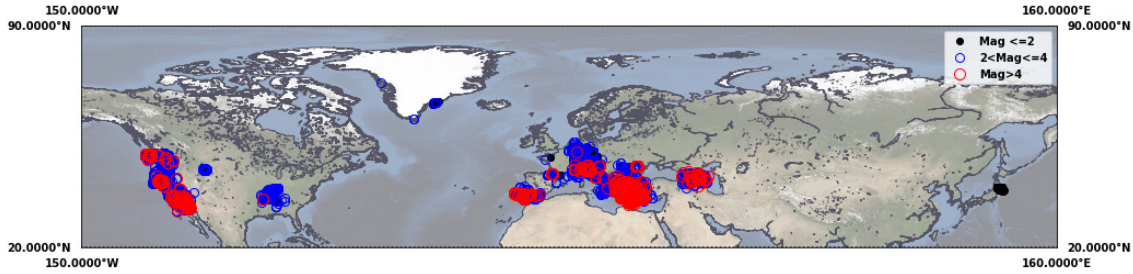
Fig. 4. Seismic map for all the tested waveforms, i.e., Southern California, western United States, European, and Japanese seismic data. The black dots are the earthquakes having a magnitude below 2 Ml, while the blue circles denote the events that have a magnitude between 2 and 4 Ml. The red circles represent the events that have a magnitude above 4 Ml.
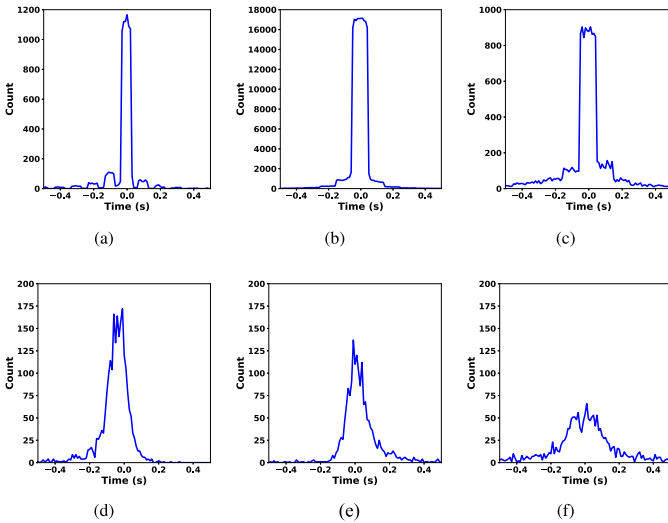

Fig. 5. PDF of the arrival time error. (a) Southern California seismic data. (b) PBO Borehole seismic data. (c) Europe seismic data. (d) Japanese seismic data (CapsNet). (e) Japanese seismic data (GPD). (f) Japanese seismic data (STA/LTA).

respectively. On the other hand, the GPD detects 1741 waveforms with an arrival time error below 0.5 s, which gives an accuracy of 76.09%; 1604 waveforms detected by the GPD have an arrival time error below 0.2 s (92.13% from the correct picked events), while 1385 waveforms have an arrival time error below 0.1 s (79.55% from the correct picked events). The three methods did not miss any event; thus, the recall of the three methods is 100%. The precision for the STA/LTA, GPD, and CapsNet is 72.84%, 76.09%, and 98.25%, respectively, while the F1-score for the STA/LTA, GPD, and CapsNet is 84.28%, 86.42%, and 99.11%, respectively. The differences between the STA/LTA picks and the manual picks have a mean value, standard deviation, mean absolute error, and mean absolute percentage error of 0.10 s, 0.80 s, 0.0381 s, and 5.29%, respectively. While the differences between the GPD picks and the manual picks have a mean value, standard deviation, mean absolute error, and mean absolute percentage error are 0.05 s, 0.10 s, 0.069 s, and 2.26%, respectively. The differences between the CapsNet picks and the manual picks have a mean value, standard deviation, mean absolute error, and mean absolute percentage error of −0.05 s, 0.082 s, 0.067 s, and 0.25%, respectively. For all the methods, the input waveform is bandpass filtered between 2 and 20 Hz. Afterward, we try several parameters of the STA/LTA and GPD to find the best

performance. Accordingly, we use an STA window of five samples and an LTA window of 15 samples, while we use a threshold of 0.95 for the GPD output probability. Table III summarizes the results' comparison of the Japanese seismic data. Accordingly, we can conclude that CapsNet has the best accuracy and outperforms the benchmark methods.

IV. DISCUSSION

A. Generalization of CapsNet

To evaluate the generalization ability of the CapsNet, we train multiple CapsNet models using different training/testing splitting rates, e.g., 10%, 30%, 50%, 70%, and 90% of the Southern California seismic data, and compare the CapsNet results to two deep learning models. The first model consists of nine blocks, each containing a fully connected neural network (FCNN) and an activation function layer. The number of the neurons per layer is 600, 300, 150, 75, 37, 18, 9, 4, and 1, respectively. The second model is based on CNN, which consists of eight blocks, each containing a convolutional, activation, and max-pooling layer. The number of feature maps per layer is 6, 12, 24, 48, 96, 96, 96, and 96, respectively. The kernel size is 3×3 for all the convolutional layers, while each max-pooling layer reduced its input dimension by 2. The input size of the CNN model is $400 \times 3 \times 1$, while the FCCN input size is 1200. The FCNN model has 961 087 network parameters, while the CNN model has 305 305 network parameters. ReLU is utilized as an activation function for both FCNN and CNN models. The training process is terminated if the training accuracy does not increase for five consecutive epochs or the number of epochs reaches 20. Table IV shows the training, and testing accuracies of the three models, i.e., FCNN, CNN, and CapsNet, using the five different training/testing splitting rates. Here, we report the testing accuracies corresponding to the training ratios for each model. The three models show high classification accuracy for the training sets. However, the FCNN starts to overfit when the training/testing rate becomes less than 50%. In this case, the FCNN testing accuracy reaches 96.75%. In addition, the FCNN loses its ability to classify the testing sets when the training ratio becomes 10%, and the testing accuracy is 94.31%. On the other hand, CNN has a more robust performance than the FCNN, and the CNN testing accuracy is 98.02% when the training ratio is 50%. However, the CNN testing accuracy started to gets below 98.00% when the

TABLE II

DISTRIBUTION OF THE CAPSNET ARRIVAL TIME ERROR FOR DIFFERENT DATASETS

Dataset	Total Events	missing events	Picking events below arrival time error of 0.5s	Accuracy	Picking events below arrival time error of 0.2s	Picking events below arrival time error of 0.1s	Precision	Recall
Southern California	8,633	57	8,331	96.50%	7,924 (95.11%)	7,280 (87.38%)	97.14%	99.32%
Western United States	196,986	181	193,368	98.16%	188,823 (97.62%)	178,911 (92.50%)	98.25%	99.90%
European	14,488	129	13,358	92.20%	11,609 (86.90%)	9,926 (74.62%)	93.03%	99.04%

TABLE III

ARRIVAL TIME DISTRIBUTION ERROR USING DIFFERENT METHODS (JAPANESE SEISMIC DATA)

Dataset	Total Events	Picking events below arrival time error of 0.5s	Accuracy	Picking events below arrival time error of 0.2s	Picking events below arrival time error of 0.1s
CapsNet	2,288	2,248	98.25%	2,142 (95.28%)	1,851 (82.33%)
GPD	2,288	1,741	76.09%	1,604 (92.13%)	1,385 (79.55%)
STA/LTA	2,288	1,666	72.84%	1,320 (57.72%)	938 (41.01%)

TABLE IV

RESULT COMPARISON OF FCNN, CNN, AND CAPSNET MODELS USING DIFFERENT TRAINING/TESTING SPLITTING RATES OF THE SOUTHERN CALIFORNIA SEISMIC DATA (4.5 MILLION 4-S-THREE-COMPONENT SEISMOGRAMS)

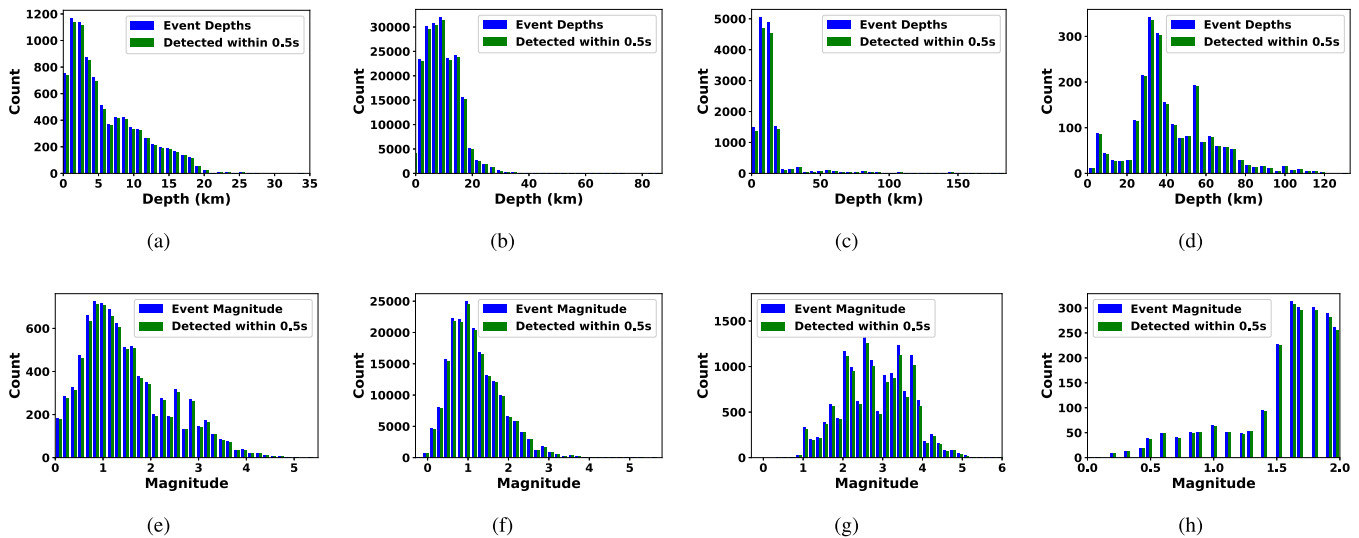| Method	Training ratio					Testing ratio				
	Training accuracy					Testing accuracy				
FCNN	10%	30%	50%	70%	90%	90%	70%	50%	30%	10%
	98.70%	98.69%	98.68%	98.68%	98.69%	94.31%	95.46%	96.75%	97.00%	97.23%
CNN	10%	30%	50%	70%	90%	90%	70%	50%	30%	10%
	98.91%	98.85%	98.73%	98.73%	98.72%	97.21%	97.48%	98.02%	98.35%	98.40%
CapsNet	10%	30%	50%	70%	90%	90%	70%	50%	30%	10%
	98.92%	98.84%	98.75%	98.74%	98.73%	98.15%	98.35%	98.42%	98.48%	98.51%

Fig. 6. Tested earthquakes parameters. The depth distribution of (a) the Southern California seismic data, (b) the western United States seismic data, (c) the European seismic data, and (d) the Japanese seismic data. The Magnitude distribution of (e) the Southern California seismic data, (f) the western United States seismic data, (g) the European seismic data, and (h) the Japanese seismic data. The green bars represent the detected earthquakes using CapsNet with an arrival time error below 0.5 s.

training ratio gets lower than 50%. CNN has testing accuracy of 97.48%, and 97.21% for the training ratio of 30%, and 10%, respectively. On the contrary, the CapsNet has a better generalization ability than FCNN and CNN, e.g., being less overfitting. CapsNet reaches testing accuracy of 98.35%, and 98.15% for the training ratio of 30%, and 10%, respectively. From these results, we can conclude that the CapsNet can learn effectively from a small dataset, which gives a better
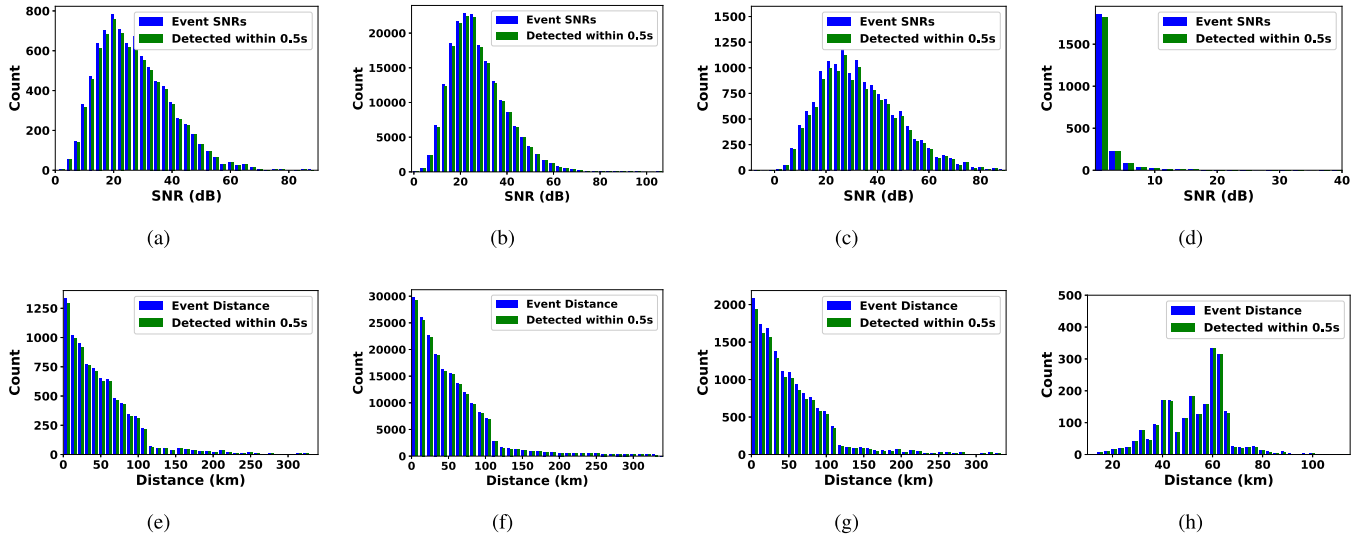
Fig. 7. Tested earthquakes parameters. The SNR distribution of (a) the Southern California seismic data, (b) the western United States seismic data, (c) the European seismic data, and (d) the Japanese seismic data. The event distance distribution of (e) the Southern California seismic data, (f) the western United States seismic data, (g) the European seismic data, and (h) the Japanese seismic data. The green bars represent the detected earthquakes using CapsNet with an arrival time error below 0.5 s.

generalization performance compared with the FCNN and CNN models. However, one of the main drawbacks of the CapsNet is that it has a longer training time than the FCNN and CNN because it includes an iteration process in its architecture, e.g., when the training/testing rate is 90%. The CNN takes 16 min to finish one epoch, while the CapsNet consumes 59 min for one epoch. These results have been reported using a laptop of Intel Processor Core i7-7700HQ CPU at 2.80 GHz, RAM of 16 Gb, and windows 10, 64-bit Operating System. CapsNet has a simple architecture, i.e., 285 504 parameters with effective identification and detection performance. It is trained using 50% of the Southern California seismic data. It shows a great generalization ability for earthquake detection and P-wave picking, i.e., it is trained using the seismic data in the Southern California area and shows a robust performance when it is tested using the seismic data in different seismic areas, e.g., western United States, Europe, and Japan areas. On the other hand, GPD [26] is one of the robust picking algorithms based on CNN, and it is trained using 75% of the Southern California seismic data with 1 742 763 network parameters in total. However, when both methods (CapsNet and GPD) are applied to the seismic data in the Japanese, the CapsNet outperforms the GPD. The CapsNet picking accuracy is 98.25%, while the picking accuracy of GPD is 76.09%. This result indicates the capability of the CapsNet in extracting more robust features from smaller training dataset without manipulation of the training data, e.g., data augmentation. However, CNN needs to be trained using a much larger dataset to extract more robust features without losing important information. CapsNet is tested using data from several seismically active areas across the planet. Besides, it is tested using various earthquakes parameters, e.g., depth and magnitude. The depth and magnitude distribution of the tested earthquakes are shown in Fig. 6. The CapsNet shows robust performance in earthquake detection regardless of the depth and the magnitude of the earthquake. In addition, we estimate the average signal-to-noise ratio (SNR) of the three-component seismogram for

each tested record and plot the distribution of the average SNRs in Fig. 7. The green bars in Figs. 6 and 7 represent the detected earthquakes using CapsNet with an arrival time error below 0.5 s. Here, the arrival time error is estimated using the mean absolute difference between the manual pick and the CapsNet pick. We can notice that the CapsNet detects most of the earthquakes despite the existence of a high background noise level. The lowest SNRs detected by the CapsNet are 1.11, −0.70, −8.07, and 0.51 dB for the Southern California, western United States, European, and Japanese seismic data, respectively. We define the SNR as follows:

$$\text{SNR} = 10 \log_{10} \frac{\|\mathbf{S}\|_2^2}{\|\mathbf{N}\|_2^2} \tag{11}$$

where S and N are 95th percentile of amplitudes in a short window after S and prior to the P arrival time, respectively [39]. Four examples of the detected first arrival time using CapsNet from Southern California, western United States, Europe, and Japan are shown in Fig. 8. The SNRs of the four examples are 3.06, −0.70, −8.07, and 0.73 dB, respectively. For the four examples in Fig. 8, the absolute differences between the manual pick and the CapsNet pick are 0.07, 0.03, 0.0, and 0.01 s, respectively. CapsNet is tested using 222 395 earthquake waveforms from different seismic areas. CapsNet misses 367 events, and the number of the events that have an arrival time error below 0.5 s is 217 305 (accuracy of 97.71%). Among them, 210 498 waveforms (96.86% from the correct picked waveforms) have an arrival time error below 0.2 s and 197 968 waveforms (91.11% from the correct picked waveforms) have an arrival time error below 0.1 s. The precision, recall, and F1-score for the CapsNet are 97.78%, 99.83%, and 98.79%, respectively.

B. Application of CapsNet to the Arkansas Microearthquakes Swarm

For further evaluation of the CapsNet, we use the seismic data recorded by station $WHAR$ in Guy-Greenbrier,
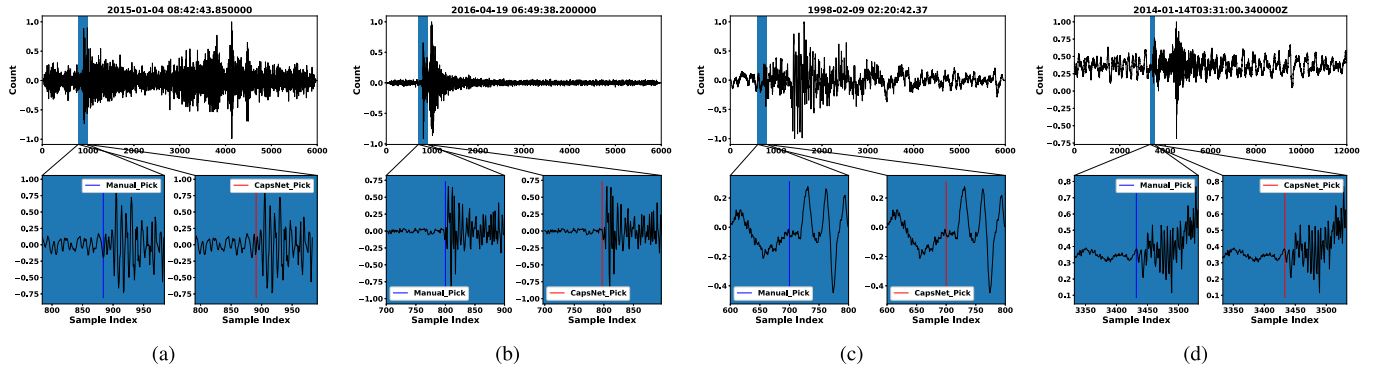
Fig. 8. Several examples of first arrival time detection using CapsNet for (a) the Southern California seismic data, (b) the western United States seismic data, (c) European seismic data, and (d) Japanese seismic data.

Arkansas [41]. We test the CapsNet using 24 h of continuous data starting from August 1, 2010. These data are microearthquakes swarm associated with a waste-water injection or hydraulic fracturing [41]. We first filter the seismic data using a bandpass filter between 2 and 20 Hz. Afterward, we divide the filtered data into several overlapping windows, each consisting of a 4-s-three-component. Then, we identify and detect the microearthquakes using CapsNet. Here, we use the output threshold to be 0.9 instead of 0.8 to avoid false alarms. Finally, we compare the picking time corresponding to the CapsNet to the unified catalog [10], [32], [41]–[43] of the Arkansas seismic data. If we found the picked time in the unified catalog, we consider this pick as a true positive. Accordingly, CapsNet releases 258 alarms for the existence of earthquakes. Among them, 155 are reported in the unified catalog. We visually check the remaining 103 alarms and find that 66 alarms are earthquakes that are not included in the unified catalog. In this case, the CapsNet detects 221 earthquakes and has 37 false alarms with a detection accuracy of 85.65%. The CapsNet successfully detects a microearthquake with a small magnitude, i.e., as low as -1.3 Ml. Fig. 9 shows an example from the Arkansas seismic data, and the first arrival triggers corresponding to CapsNet.

C. False Alarms Rate

To test the false alarms released by the CapsNet, we use 100 000 60-s-three-component noise waveforms from the STEAD dataset [39]. The tested noise waveforms are recorded by different seismic stations from different seismic networks worldwide. Each waveform is band-bass filtered between 2 and 20 Hz and divided into several 4-s-three-component overlapped windows. Afterward, CapsNet obtains the class of each window and decides whether there is an earthquake. The output threshold is set to be 0.8 (the default value). As a result, the CapsNet releases 1384 false alarms from a total of 100 000 waveforms, which gives a CapsNet accuracy of 98.61%. We can reduce the false alarms rate by increasing the output threshold to be 0.9, which would probably result in more missed earthquakes.

D. Effect of the Sampling Rate

CapsNet is trained and tested using seismic data with a sampling rate of 100 Hz. For higher sample rates, the first
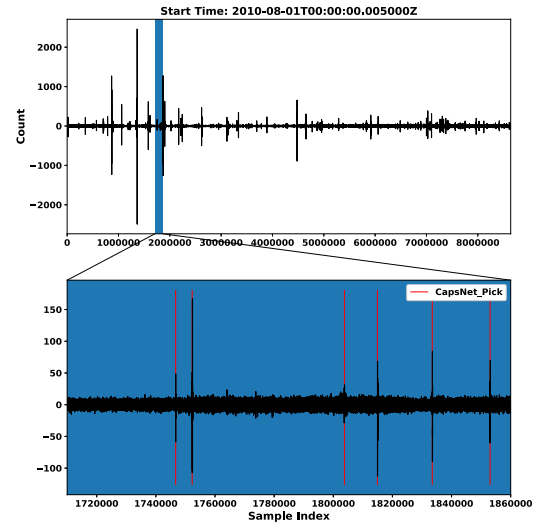

Fig. 9. CapsNet triggering in the microearthquakes swarm case (Arkansas seismic data).

step is to downsample the input data to reach a 100-Hz sampling rate. However, it becomes more challenging when the sample rate is lower than 100 Hz. In this case, the input seismic data should be interpolated to reach a 100-Hz sampling rate. CapsNet has been evaluated using Texas seismic data [44] recorded by station US.MNTX between January 1, 2017, till the end of May 2018. The first arrival time of the tested waveforms has been extracted from the TexNet seismic catalog [44]. Accordingly, 288 earthquakes are tested with a magnitude range of 1.5 and 2.8 Ml, and the depth varies from 0 to 10.4 km. The event distance range varies from 57.77 to 154.40 km. The sampling rate of station US.MNTX is 40 Hz, and we first interpolate the seismic data and bandpass filtered between 2 and 20 Hz. Afterward, CapsNet is applied to the 4-s-three-component windows to detect the first arrival time and compare it to the TexNet seismic catalog. The CapsNet detects more than 94.00% of the tested waveforms (272 events) within 0.5-s arrival time error. However, CapsNet does not show a precise picking performance, and only 201 events (73.89% from the correct picked waveforms) are within 0.2-s arrival time error, while 113 events have an arrival time error below 0.1 s. The CapsNet precision, recall, and F1-score are 94.44%, 100%, and 97.14%, respectively.

E. Drawbacks of the Proposed Algorithm

The output label for the CapsNet is one for both P- and S-waves' windows and zero for noise windows. However, this methodology makes the decision difficult when the detected high-probabilities are related to P- or S-wave because both are included in the same output signal. In normal scenarios, the P-wave will be followed by the S-wave; thus, we assume that the first detected peak is related to the P-wave, and the second is related to the S-wave. However, this assumption will produce false alarms in the case when the two peaks are related to the S-waves when the emergent P-waves of events are below the noise level or when two different events are next to each other. To solve this problem, we train a new CapsNet model with the same architecture, where the output labels are one for the P-wave windows and zero for both S-wave and noise windows. In such a case, the output probability will be very high for the P-wave window and almost zero for the S-wave and noise windows. We train the new CapsNet model using 50% of the Southern California dataset, 25% for validation, and 25% for testing. As a result, the training accuracy reaches 98.80%, while the validation and testing accuracies are 98.49% and 98.46%, respectively; 20 epochs are used to finish the training process. After 12 epochs, the validation accuracy did not enhance. In this model, detection of probability higher than 0.8 refers to the existence of P-wave (earthquake). Thus, the output signal of the new model contains only one peak related to the P-wave. Afterward, the new CapsNet model is applied to the Japanese dataset. As a result, the new CapsNet model detects 2246 waveforms that give an accuracy of 98.23%. Among the correctly detected waveforms, 2136 waveforms have an arrival time error below 0.2 s (95.10% from the correct picked events), and 1840 events have an arrival time error below 0.1 s (81.90% from the correct picked events). The results of the new CapsNet model are similar to the old CapsNet model (having two peaks related to the P- and S-waves). The new CapsNet model (having only one peak related to the P-wave) can be applied independently, in which the detection and identification of the earthquakes are related to the existence of the P-wave. However, this new CapsNet model can be merged with the old CapsNet model (having two peaks related to the P- and S-waves). Every detected peak from the old CapsNet model can be checked whether it exists in the output of the new CapsNet model. If this is the case, it means that this peak is related to the P-wave; otherwise, it refers to S-wave. In this way, the drawback of the current framework can be mitigated. We applied this methodology on the Japanese seismic data. First, we obtain the output probability of the old and new CapsNet models. Second, we check the matching peak between the two output probabilities and consider it as the P-wave arrival time. Third, we obtain the S-wave arrival time from the second peak of the output probability of the old CapsNet model. As a result, the S-wave picking accuracy reaches 87.23% (2156 waveforms within 0.5-s arrival time error). Among the correctly detected waveforms, 1897 waveforms have an arrival time error below 0.2 s (87.99% from the picked events) and 1360 events have an arrival time error below 0.1 s. We can notice that the CapsNet does not provide a precise S-wave picking; it just helps the model to identify the

earthquake by the existence of the two peaks related to the P- and S-waves. Therefore, for future work, we will investigate the false alarms produced by the CapsNet and figure out the source of errors for further enhancement of the proposed algorithm. In addition, we aim to design a CapsNet model with two separate outputs related to P- and S-waves, respectively. In this way, we can detect and classify the seismic phase independently with a robust picking performance.

V. Conclusion

We have proposed a robust earthquake identification and detection method based on a CapsNet. CapsNet is the next generation of deep learning architectures, allowing the network to extract more robust features without losing important information. CapsNet has the ability to obtain a robust generalization performance by learning from a small dataset. CapsNet is designed to identify the earthquake signals in the seismic noise and detect the first arrival time of the earthquake. CapsNet is trained using 50% of the Southern California seismic data, which consists of 4.5 million 4-s-three-component seismograms and tested using 222 395 waveforms from different seismic areas, e.g., western United States, Europe, and Japan. CapsNet shows a robust detection performance, identifying and detecting 217 305 events, and misses 367 events. More than 97% of the correctly picked waveforms have an arrival time error below 0.2 s and 91.11% of the correct picked waveforms within an arrival time error of 0.1 s. CapsNet has been applied to one-day continuous data associated with a microearthquakes swarm that happened in Arkansas. It detects 211 earthquakes and releases 37 false alarms with a detection accuracy of 85.01%. CapsNet is compared with benchmark methods, e.g., STA/LTA and GPD methods, and outperforms them. However, the CapsNet does not perform equally well on data with sampling rates lower than 100 Hz.

Data Availability

The Southern California seismic data are open-source data that can be found in [26]. Arkansas datasets are open-source dataset that can be found in [41]. The STEAD data can be downloaded from [39]. The Texas dataset can be downloaded via http://service.iris.edu/fdsnws/dataselect/1/. The Japanese dataset can be requested and downloaded via (https://www.jma.go.jp/jma).
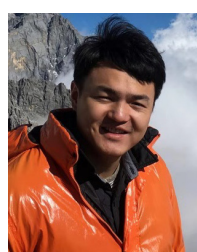
References

[1] R. V. Allen, "Automatic earthquake recognition and timing from single traces," *Bull. Seismological Soc. Amer.*, vol. 68, no. 5, pp. 1521–1532, 1978.

[2] M. Leonard and B. L. N. Kennett, "Multi-component autoregressive techniques for the analysis of seismograms," *Phys. Earth Planet. Interiors*, vol. 113, nos. 1–4, pp. 247–263, Jun. 1999.

[3] Y. Chen, "Automatic microseismic event picking via unsupervised machine learning," *Geophys. J. Int.*, vol. 222, no. 1, pp. 1750–1764, 2020.

[4] Y. Chen, "Fast waveform detection for microseismic imaging using unsupervised machine learning," *Geophys. J. Int.*, vol. 215, no. 2, pp. 1185–1199, Nov. 2018.

[5] Z. Li, Z. Peng, D. Hollis, L. Zhu, and J. McClellan, "High-resolution seismic event detection using local similarity for large-N arrays," *Sci. Rep.*, vol. 8, no. 1, p. 1646, Dec. 2018.

[6] K. J. Bergen and G. C. Beroza, "Earthquake fingerprints: Extracting waveform features for similarity-based earthquake detection," *Pure Appl. Geophys.*, vol. 176, no. 3, pp. 1037–1059, Mar. 2019.

[7] S. Qu, Z. Guan, E. Verschuur, and Y. Chen, "Automatic high-resolution microseismic event detection via supervised machine learning," *Geophys. J. Int.*, vol. 222, no. 3, pp. 1881–1895, 2020.

[8] D. Zhu, Y. Li, and C. Zhang, "Automatic time picking for microseismic data based on a fuzzy C-means clustering algorithm," *IEEE Geosci. Remote Sens. Lett.*, vol. 13, no. 12, pp. 1900–1904, Dec. 2016.

[9] A. G. Hafez, M. Rabie, and T. Kohda, "Seismic noise study for accurate P-wave arrival detection via MODWT," *Comput. Geosci.*, vol. 54, pp. 148–159, Apr. 2013.

[10] C. E. Yoon, O. O'Reilly, K. J. Bergen, and G. C. Beroza, "Earthquake detection through computationally efficient similarity search," *Sci. Adv.*, vol. 1, no. 11, Dec. 2015, Art. no. e1501057.

[11] A. Lomax, A. Michelini, and D. Jozinović, "An investigation of rapid earthquake characterization using single-station waveforms and a convolutional neural network," *Seismological Res. Lett.*, vol. 90, no. 2A, pp. 517–529, 2019.

[12] J. El Zini, Y. Rizk, and M. Awad, "A deep transfer learning framework for seismic data analysis: A case study on bright spot detection," *IEEE Trans. Geosci. Remote Sens.*, vol. 58, no. 5, pp. 3202–3212, May 2020.

[13] W. Zhu, S. M. Mousavi, and G. C. Beroza, "Seismic signal denoising and decomposition using deep neural networks," *IEEE Trans. Geosci. Remote Sens.*, vol. 57, no. 11, pp. 9476–9488, Nov. 2019.

[14] Z. Gao, Z. Pan, C. Zuo, Z. Gao, and Z. Xu, "An optimized deep network representation of multimutation differential evolution and its application in seismic inversion," *IEEE Trans. Geosci. Remote Sens.*, vol. 57, no. 7, pp. 4720–4734, Jul. 2019.

[15] Y. Wu, Y. Lin, Z. Zhou, D. C. Bolton, J. Liu, and P. Johnson, "DeepDetect: A cascaded region-based densely connected network for seismic event detection," *IEEE Trans. Geosci. Remote Sens.*, vol. 57, no. 1, pp. 62–75, Jan. 2019.

[16] X. Chai, G. Tang, S. Wang, R. Peng, W. Chen, and J. Li, "Deep learning for regularly missing data reconstruction," *IEEE Trans. Geosci. Remote Sens.*, vol. 58, no. 6, pp. 4406–4423, Jun. 2020.

[17] S. M. Mousavi, W. L. Ellsworth, W. Zhu, L. Y. Chuang, and G. C. Beroza, "Earthquake transformer—An attentive deep-learning model for simultaneous earthquake detection and phase picking," *Nature Commun.*, vol. 11, no. 1, pp. 1–12, 2020.

[18] X. Wu, Y. Shi, S. Fomel, L. Liang, Q. Zhang, and A. Z. Yusifov, "FaultNet3D: Predicting fault probabilities, strikes, and dips with a single convolutional neural network," *IEEE Trans. Geosci. Remote Sens.*, vol. 57, no. 11, pp. 9138–9155, Nov. 2019.

[19] G. Zhang, Z. Wang, and Y. Chen, "Deep learning for seismic lithology prediction," *Geophys. J. Int.*, vol. 215, pp. 1368–1387, Aug. 2018.

[20] O. M. Saad and Y. Chen, "Deep denoising autoencoder for seismic random noise attenuation," *Geophysics*, vol. 85, no. 4, pp. V367–V376, Jul. 2020.

[21] O. Saad and Y. Chen, "Automatic waveform-based source-location imaging using deep learning extracted microseismic signals," *Geophysics*, vol. 85, no. 6, 2020, Art. no. doi: 10.1190/geo2020-0288.1.

[22] S. Li *et al.*, "Deep-learning inversion of seismic data," *IEEE Trans. Geosci. Remote Sens.*, vol. 58, no. 3, pp. 2135–2149, Mar. 2020.

[23] G. Zhang, C. Lin, and Y. Chen, "Convolutional neural networks for microseismic waveform classification and arrival picking," *Geophysics*, vol. 85, no. 4, pp. WA227–WA240, Jul. 2020.

[24] S. M. Mousavi, W. L. Ellsworth, W. Zhu, L. Y. Chuang, and G. C. Beroza, "Earthquake transformer—An attentive deep-learning model for simultaneous earthquake detection and phase picking," *Nature Commun.*, vol. 11, no. 1, pp. 1–12, 2020.

[25] W. Zhu and G. C. Beroza, "PhaseNset: A deep-neural-network-based seismic arrival-time picking method," *Geophys. J. Int.*, vol. 216, no. 1, pp. 261–273, 2018.

[26] Z. E. Ross, M. Meier, E. Hauksson, and T. H. Heaton, "Generalized seismic phase detection with deep learning," *Bull. Seismological Soc. Amer.*, vol. 108, no. 5A, pp. 2894–2901, Oct. 2018.

[27] T. Perol, M. Gharbi, and M. Denolle, "Convolutional neural network for earthquake detection and location," *Sci. Adv.*, vol. 4, no. 2, Feb. 2018, Art. no. e1700578.

[28] O. M. Saad, K. Inoue, A. Shalaby, L. Samy, and M. S. Sayed, "Automatic arrival time detection for earthquakes based on stacked denoising autoencoder," *IEEE Geosci. Remote Sens. Lett.*, vol. 15, no. 11, pp. 1687–1691, Nov. 2018.

[29] P. M. DeVries, F. Viégas, M. Wattenberg, and B. J. Meade, "Deep learning of aftershock patterns following large earthquakes," *Nature*, vol. 560, no. 7720, pp. 632–634, 2018.

[30] Z. E. Ross, M.-A. Meier, and E. Hauksson, "*P* wave arrival picking and first-motion polarity determination with deep learning," *J. Geophys. Res. Solid Earth*, vol. 123, no. 6, pp. 5120–5129, 2018.

[31] Z. E. Ross, Y. Yue, M. Meier, E. Hauksson, and T. H. Heaton, "PhaseLink: A deep learning approach to seismic phase association," *J. Geophys. Res. Solid Earth*, vol. 124, no. 1, pp. 856–869, Jan. 2019.

[32] S. M. Mousavi, W. Zhu, Y. Sheng, and G. C. Beroza, "CRED: A deep residual network of convolutional and recurrent units for earthquake signal detection," *Sci. Rep.*, vol. 9, no. 1, pp. 1–14, Dec. 2019.

[33] S. Sabour, N. Frosst, and G. E. Hinton, "Dynamic routing between capsules," in *Proc. Adv. Neural Inf. Process. Syst.*, 2017, pp. 3856–3866.

[34] B. Jia and Q. Huang, "De-capsnet: A diverse enhanced capsule network with disperse dynamic routing," *Appl. Sci.*, vol. 10, no. 3, p. 884, 2020.

[35] M. D. Zeiler and R. Fergus, "Visualizing and understanding convolutional networks," in *Proc. Eur. Conf. Comput. Vis.* Springer, 2014, pp. 818–833.

[36] Z. He, P. Peng, L. Wang, and Y. Jiang, "PickCapsNet: Capsule network for automatic P-wave arrival picking," *IEEE Geosci. Remote Sens. Lett.*, early access, Apr. 4, 2020, doi: 10.1109/LGRS.2020.2983196.

[37] R. Mukhometzianov and J. Carrillo, "CapsNet comparative performance evaluation for image classification," 2018, *arXiv:1805.11195*. [Online]. Available: http://arxiv.org/abs/1805.11195

[38] D. P. Kingma and J. Ba, "Adam: A method for stochastic optimization," 2014, *arXiv:1412.6980*. [Online]. Available: http://arxiv.org/abs/1412.6980

[39] S. M. Mousavi, Y. Sheng, W. Zhu, and G. C. Beroza, "Stanford Earthquake Dataset (STEAD): A global data set of seismic signals for AI," *IEEE Access*, vol. 7, pp. 179464–179476, 2019.

[40] (2020). *Japan Meteorological Agency*. Accessed: May 23, 2020. [Online]. Available: https://www.jma.go.jp/jma

[41] S. Horton, "Disposal of hydrofracking waste fluid by injection into subsurface aquifers triggers earthquake swarm in central arkansas with potential for damaging earthquake," *Seismological Res. Lett.*, vol. 83, no. 2, pp. 250–260, Mar. 2012.

[42] Y. Huang and G. C. Beroza, "Temporal variation in the magnitude-frequency distribution during the guy-greenbrier earthquake sequence," *Geophys. Res. Lett.*, vol. 42, no. 16, pp. 6639–6646, Aug. 2015.

[43] P. O. Ogwari, S. P. Horton, and S. Ausbrooks, "Characteristics of induced/triggered earthquakes during the startup phase of the Guy–Greenbrier earthquake sequence in north–central Arkansas," *Seismological Res. Lett.*, vol. 87, no. 3, pp. 620–630, May 2016.

[44] A. Savvaidis, B. Young, G.-C. D. Huang, and A. Lomax, "TexNet: A statewide seismological network in Texas," *Seismological Res. Lett.*, vol. 90, no. 4, pp. 1702–1715, 2019.

Omar M. Saad received the B.S. and M.S. degrees in electrical engineering from the Arab Academy for Science, Technology & Maritime Transport (AASTMT), Alexandria, Egypt, in 2012 and 2015, respectively, and the Ph.D. degree in electrical engineering from the Egypt Japan University of Science and Technology (EJUST), Alexandria, in 2019.

He is a Researcher with the National Research Institute of Astronomy and Geophysics (NRIAG), Helwan, Egypt. He also holds a post-doctoral position at the School of Earth Sciences, Zhejiang University, Hangzhou, China. He is mainly engaged in machine learning in the field of seismology, earthquake early warning systems, and signal processing techniques.

Yangkang Chen received the B.S. degree in exploration geophysics from the China University of Petroleum, Beijing, China, in 2012, and the Ph.D. degree in geophysics from The University of Texas at Austin, Austin, TX, USA, in 2015, under the supervision of Prof. S. Fomel.

From 2016 to 2018, he was a Distinguished Post-Doctoral Research Associate with the Oak Ridge National Laboratory, Oak Ridge, TN, USA. He is an Assistant Professor with Zhejiang University, Hangzhou, China. He has authored more than 100 internationally renowned journal articles and more than 80 international conference papers. His research interests include seismic signal analysis, seismic modeling and inversion, simultaneous-source data deblending and imaging, global adjoint tomography, and high-performance computing.